

A Surprising Reversal of Temperatures in the Brown-Dwarf Eclipsing Binary 2MASS J05352184–0546085

Keivan G. Stassun¹, Robert D. Mathieu², and Jeff A. Valenti³

ABSTRACT

The newly discovered brown-dwarf eclipsing binary 2MASS J05352184–0546085 provides a unique laboratory for testing the predictions of theoretical models of brown-dwarf formation and evolution. The finding that the lower-mass brown dwarf in this system is hotter than its higher-mass companion represents a challenge to brown-dwarf evolutionary models, none of which predict this behavior. Here we present updated determinations of the basic physical properties of 2M0535–05, bolstering the surprising reversal of temperatures with mass in this system. We compare these measurements with widely used brown-dwarf evolutionary tracks, and find that the temperature reversal can be explained by some models if the components of 2M0535–05 are mildly non-coeval, possibly consistent with dynamical simulations of brown-dwarf formation. Alternatively, a strong magnetic field on the higher-mass brown dwarf might explain its anomalously low surface temperature, consistent with emerging evidence that convection is suppressed in magnetically active, low-mass stars. Finally, we discuss future observational and theoretical work needed to further characterize and understand this benchmark system.

Subject headings: stars: low mass, brown dwarfs—binaries: eclipsing—stars: fundamental parameters—stars: formation—stars: individual (2MASS J05352184–0546085)

1. Introduction

Born with masses between the least massive stars ($\approx 0.072 M_{\odot}$; Chabrier & Baraffe 2000) and the most massive planets ($\approx 0.013 M_{\odot}$; Burrows et al. 2001), brown dwarfs at once extend our understanding of the formation and evolution of both stars and planets. In the decade since the discovery of the first brown dwarfs (Nakajima et al. 1995; Rebolo et al. 1995), the study of star- and planet-formation has increasingly trained its attention on these objects that, while being neither star nor planet, may provide key insights to understanding the origins of both (Basri 2000).

Such an understanding must be founded on accurate measurements of fundamental physical properties—masses, radii, and luminosities. Unfortunately, the number of objects for which these properties can be measured directly is extremely small. Though rare, eclipsing binaries have long been employed as ideal laboratories for directly measuring fundamental stellar parameters (e.g. Andersen 1991). The power of eclipsing binaries lies in their provision of masses and radii with only the most basic of theoretical assumptions. With the addition of atmosphere models the ratio of effective temperatures can also be derived, and luminosities

¹Department of Physics & Astronomy, Vanderbilt University, Nashville, TN 37235; keivan.stassun@vanderbilt.edu

²Department of Astronomy, University of Wisconsin–Madison, Madison, WI, 53706

³Space Telescope Science Institute, Baltimore, MD 21218

can then be determined directly through the Stefan-Boltzmann law without knowledge of distance. Finally, considering the two objects’ properties together permits study of the binary as twins at birth whose evolutionary histories differ because of their different masses.

Thus the recent discovery of a brown-dwarf eclipsing binary system in the Orion Nebula Cluster, 2MASS J05352184–0546085 (hereafter 2M0535–05), offers a unique laboratory with which to directly and accurately test the predictions of theoretical models of brown-dwarf formation and evolution (Stassun, Mathieu, & Valenti 2006, hereafter Paper I). In Paper I, we presented a preliminary analysis of the orbit and of the mutual eclipses in 2M0535–05 to directly measure the masses and radii of both components, as well as the ratio of their effective temperatures. Our mass measurements reveal both objects in this young binary system to be substellar, with masses of $M_1 = 55 M_{\text{Jup}}$ and $M_2 = 35 M_{\text{Jup}}$, accurate to $\sim 10\%$. In addition, from the observed eclipse durations and orbital velocities we directly measured the radii of the brown dwarfs to be $R_1 = 0.67 R_{\odot}$ and $R_2 = 0.51 R_{\odot}$, accurate to $\sim 5\%$, and representing the first direct measurements of brown-dwarf radii. Such large radii are generally consistent with theoretical predictions of young brown dwarfs in the earliest stages of gravitational contraction.

Surprisingly, however, we reported in Paper I that the lower-mass brown dwarf has an effective temperature that is slightly—but significantly—warmer than its higher-mass companion. Such a reversal of temperatures with mass is not predicted by any theoretical model for coeval brown dwarfs. This finding has potentially important ramifications for theoretical brown-dwarf evolutionary tracks, and thus for our understanding of brown-dwarf formation more generally.

In this paper, we present supplementary light-curve and radial-velocity measurements (§2) which we use to refine our determination of the basic physical properties of 2M0535–05 (§3). We verify the finding of a temperature reversal with mass in this system, and quantitatively compare the empirically determined physical parameters with those predicted by theoretical evolutionary tracks. We then briefly explore the implications of the temperature reversal in 2M0535–05 for theoretical models of brown-dwarf formation and evolution (§4). Specifically, we consider whether the temperature reversal can be explained by dynamical brown-dwarf formation scenarios and/or by the physical effects of strong surface fields on young brown dwarfs. We summarize our conclusions in §5.

2. Data and Methods

2.1. Spectroscopic observations: Radial velocities and spectral types

We observed 2M0535–05 with the *Phoenix* spectrograph on Gemini South on eight separate nights from December 2002 to January 2003 (first reported in Paper I) and again on 03 March 2005 (newly reported here). All nine observations were obtained with the same instrument setup. Following Mazeh et al. (2002), we observed the wavelength range 1.5515–1.5585 μm (central wavelength 1.555 μm ; *H* band) at a resolving power of $R \approx 30000$ (slit size of $0''.35$). Exposure times were varied between 1.0 and 3.3 hr by the queue observers based on sky conditions. The typical exposure time was 2.6 hr (i.e. ~ 0.01 orbital phase; see §2.2), divided into 6 telescope nods in an **abbaab** pattern for the purposes of sky subtraction and cosmic-ray rejection. An observation of the CORAVEL-ELODIE high-precision radial-velocity standard HD 50778 (K4 III; Udry et al. 1999) was obtained immediately before or after each observation of 2M0535–05 to monitor the instrument wavelength zero point. In addition, observations were obtained of a grid of late-type spectral standards, with spectral types of M0 to M9, selected from Mazeh et al. (2002) and Mohanty & Basri (2003). The standard-star observations are summarized in Table 1.

The observations were processed using Interactive Data Language procedures developed specifically for optimal extraction of *Phoenix* spectra. The background subtraction step includes logic to compensate for variations in the night sky lines due to grating motion or brightness variations between nods. A bootstrap procedure is used to determine a wavelength solution from ThNeAr calibration spectra obtained immediately before and after the science exposures. First an *a priori* wavelength dispersion is determined by matching a *Phoenix* spectrum of a K giant with the KPNO FTS atlas of Arcturus (Hinkle et al. 1995). Next, a small wavelength shift (less than 1 km s^{-1}) is applied to match the mean wavelengths of the three strongest ThNeAr lines as a function of position along the slit. Finally, a multi-Gaussian fit is used to empirically determine the wavelengths of the remaining ThNeAr lines. The individual exposures from the different slit positions are combined and interpolated onto a uniform dispersion and then continuum normalized using sixth-order polynomial fits to the high points in the spectra. Typical signal-to-noise ratios of the extracted spectra were ~ 15 per resolution element for the nine observations of 2M0535–05 and ~ 50 per resolution element for the standard stars.

Absolute heliocentric radial velocities of the late-type standards were determined relative to the CORAVEL-ELODIE standard star HD 50778 (see above). To minimize the possibility of introducing systematic velocity offsets due to large differences in spectral type between this K4 standard and the late-M standards, we applied velocity corrections in a step-wise fashion, determining the velocity shift of each sequentially later type standard by cross-correlating it with the standard from the previous step (e.g., M0 relative to K4, M1 relative to M0, and so on). The radial velocities reported below are thus formally on the CORAVEL-ELODIE system (Udry et al. 1999).

Radial velocities of the two components of 2M0535–05 were determined via the technique of Broadening Functions (BFs) described by Rucinski (1999). As discussed in that study, BFs are less prone than simple cross-correlation techniques to “peak pulling,” in which closely spaced correlation features in double-lined binaries can alter the positions of the correlation peak centroids, particularly when the velocity separation of the components is on the order of the spectral resolution. The BF analysis requires a radial-velocity template spectrum that is well matched in spectral type to the target; we determined that the M6.5 star LHS 292 from our grid of standards was the best template for this purpose (see below).

In seven of the nine *Phoenix* spectra of 2M0535–05 the BFs show two clear peaks, an example of which is shown in Fig. 1. For these seven observations, radial velocities and their uncertainties were determined using two-Gaussian fits to the BFs (e.g. Rucinski 1999). We designate the component producing the stronger peak in the BFs as the ‘primary’ and the component producing the weaker peak in the BFs the ‘secondary’ (as we show below, the primary component so defined is also the more massive of the pair). One of the remaining two observations was by chance taken during eclipse of the primary (orbital phase 0.75; see Fig. 3) and thus appears as a single-lined spectrum; the BF peak was fit with a single Gaussian and its velocity assigned to the secondary. The other observation occurs shortly after eclipse of the secondary (orbital phase 0.12) and thus appears as a blended spectrum producing a single, broadened BF peak; in this case two Gaussians were fit, their initial centroids estimated from the preliminary orbit solution of Paper I and their widths fixed based on the widths of the well-separated BF peaks from the other spectra. Radial velocities and their uncertainties so measured are summarized in Table 2 and displayed in Fig. 2.

We found that the BF peaks of both components appeared strongest when we used LHS 292, an old M6.5 dwarf (see Table 1), as the radial-velocity template in the BF analysis. The BF peaks were $\sim 20\%$ weaker when we used the M6 or M7 dwarfs as templates, and weaker still when we used earlier or later templates. This suggests that the spectral types of both components of 2M0535–05 are also $\sim M6.5$. Indeed, we found in Paper I (cf. Fig. 3 in that paper) that the isolated spectrum of the primary component of 2M0535–05

very closely matches that of LHS 292, and that the JHK colors of 2M0535–05 imply a spectral type in combined light of $M6.5\pm0.5$ with negligible reddening. Taken together, the available evidence suggests that the components of 2M0535–05 have very similar spectral types of $\sim M6.5\pm0.5$, corresponding to $T_{\text{eff}} \approx 2700$ K (Slesnick et al. 2004; Golimowski et al. 2004).

While our light-curve analysis below (§2.3) yields a T_{eff} ratio of ~ 1 , reinforcing the conclusion that the components of 2M0535–05 are very similar in spectral type, we caution that our assignment of absolute spectral types is preliminary and subject to systematic uncertainty. The differences in spectral features seen in late-M standard stars are extremely subtle for dwarfs with spectral types M4–M8 (e.g. Bender et al. 2005; Prato et al. 2002), and the low S/N of our 2M0535–05 spectra prohibits a detailed analysis of spectral features. Moreover, the low surface gravities and strong magnetic fields of young, low-mass objects can bias classification of their spectra, in the sense that the true spectral types may be 1–2 subtypes later than inferred from comparison to old, high-gravity dwarfs (Mohanty & Basri 2003). Thus, for our purposes here, we emphasize that the spectral match between 2M0535–05 and the adopted radial-velocity template is sufficiently good to permit precise radial velocity measurements, and that the spectral types of the components of 2M0535–05 are evidently very similar to one another.

Because the components of 2M0535–05 have such similar spectral types, the relative BF peak areas reflect the two components’ relative contributions to the total light of the system (e.g. Bayless & Orosz 2006). In particular, the primary component apparently contributes approximately 50% more flux than the secondary at $1.555 \mu\text{m}$ (see Fig. 1). This flux ratio provides an important additional constraint for removing degeneracies in the determination of physical parameters, as we discuss in §2.3.

The component masses that we determine in §2.3 follow directly from an orbit solution fit to the observed radial velocities, and thus the uncertainties in the derived masses (and in other properties that in turn depend on those masses) depend sensitively on uncertainties in the radial velocity measurements. The mean precisions of the radial-velocity measurements from the BF analysis are formally 1.7 and 1.9 km s^{-1} for the 2M0535–05 primary and secondary, respectively (see σ_{RV} column of Table 2). However, the accuracy of these measurements can potentially be degraded by various systematic effects. At the instrument level, the stability of the wavelength zero-point is of particular concern. To assess this, we cross-correlated the first observation of the CORAVEL-ELODIE standard star HD 50778 against each subsequent observation of this star, providing a measure of the instrument stability over the course of our *Phoenix* observations. The resulting radial velocities of HD 50778 exhibit an r.m.s. scatter of 0.45 km s^{-1} on the nights that 2M0535–05 was observed, which is much smaller than the random errors in the individual measurements of 2M0535–05. Another possible source of systematic error is spectral-type mismatch between 2M0535–05 and the radial-velocity template. However, as discussed above, the radial-velocity template that we used in the BF analysis appears to match the spectral types of the 2M0535–05 components very well. Moreover, the components of 2M0535–05 have very similar spectral types to one another, so that any systematic effects due to spectral mismatch with the template should affect both components similarly, in which case only the center-of-mass velocity will be affected.

Finally, the observed radial velocities can be affected by spots on the surfaces of the brown dwarfs that cause phase-dependent distortions in the shapes of the spectral lines, and in fact we show in §2.3.1 that spots are clearly present on one or both of the components in 2M0535–05. While the data suggest that this effect is small, we have not yet incorporated a physical spot model into our analysis and thus any spot signatures remain as potential systematics in the radial velocities. In V1174 Ori, for example, a young eclipsing binary with photometric spot amplitudes similar to those observed in 2M0535–05, we found that the resulting radial-velocity distortions were as large as $\sim 1 \text{ km s}^{-1}$ at certain orbital phases (Stassun et al. 2004a). Analyses

of other spotted, low-mass eclipsing systems find similar effects; for example, GU Boo shows distortions of $\sim 0.5 \text{ km s}^{-1}$ (López-Morales & Ribas 2005) and YY Gem shows distortions of $\sim 1 \text{ km s}^{-1}$ (Torres & Ribas 2002). Any spot-induced radial-velocity distortions in 2M0535–05 would need to be 2–3 times larger than in these systems to be comparable to the random measurement errors of $\sim 1.5\text{--}2 \text{ km s}^{-1}$ (for an example of such a system, see Neuhaeuser et al. 1998). Encouragingly, the residuals of the radial-velocity measurements with respect to the final orbit solution of §2.3 ($\chi_\nu^2 = 0.7$ and 1.2 for the primary and secondary velocities, respectively; see Table 2) do not indicate that systematic effects dominate the radial-velocity measurement errors.

2.2. Photometric observations: Light curves

We have continued to photometrically monitor 2M0535–05 intensively with the 1.0-m and 1.3-m telescopes at CTIO and, as of this writing, possess a total of 2404 I_C -band measurements spanning the time period 1994 December to 2006 April. The observing campaign to date is summarized in Table 3, and the individual measurements are provided in Table 4. We have excluded a small number of observations with photometric errors larger than 0.1 mag. Thus, photometric errors on the individual measurements have a range of 0.01–0.1 mag, with a mean error of 0.024 mag and a median error of 0.020 mag.

A period search based on the phase dispersion minimization (PDM) technique of Stellingwerf (1978) reveals an unambiguous period of $P = 9.7795557 \pm 0.000019 \text{ d}$. The PDM technique is well suited to periodic variability that is highly non-sinusoidal in nature, as is the case for most detached eclipsing binaries. This updated period is slightly shorter than, but not inconsistent with, the period reported in Paper I (see Table 5).

In Fig. 3 we show the I_C -band light curve of 2M0535–05 folded on this period. Two distinct eclipses are clearly evident and cleanly separated in phase, as is typical of fully detached eclipsing binaries. One eclipse—the ‘primary eclipse’ at orbital phase ~ 0.075 —is notably deeper than the other; this marks the time in the orbit when the hotter component is eclipsed which, as discussed in Paper I and below in §3.2, in this system is the lower-mass component.

In addition, the time from primary to secondary eclipse is longer than that from secondary to primary eclipse, indicating an eccentric orbit. More quantitatively, the two parameters that determine the shape and orientation of the orbit—the eccentricity, e , and the argument of periastron, ω —can be estimated from geometrical considerations relating the orbital period, the durations of the eclipses (6.8 hr and 10.1 hr, respectively), and their 6.5-day separation in time (e.g. Kallrath & Milone 1999), from which we estimate $e \approx 0.35$ and $\omega \approx 216^\circ$. These initial estimates of e and ω agree well with the more precise values that we obtain from detailed light-curve modeling and analysis below (§2.3; Table 5).

In addition to the extensive I_C -band light curve measurements, we have also now obtained a set of near-infrared (JHK) light curves. These are presented and analyzed in a subsequent paper (Gómez Maqueo Chew et al. 2007), but we note here that the same features observed in the I_C -band light curve are also seen at these other wavelengths.

2.3. Analysis

As in Paper I, we have performed a simultaneous analysis of the *Phoenix* radial velocities and the I_C -band light curve using the eclipsing-binary algorithms of Wilson & Devinney (1971, updated 2005; hereafter WD) as implemented in the PHOEBE code of Prša & Zwitter (2005). WD has become standard in the modeling and analysis of all manner of eclipsing binary systems, having grown in sophistication over the past 35 years to include, e.g., phase-dependent projection effects in eccentric orbits, radial-velocity perturbations arising from proximity and eclipse effects, apsidal motion, and reflection and limb-darkening effects. In its most advanced implementation, the code can also treat the effects of surface spots, model atmospheres, and asynchronous rotation, including any attendant gravity brightening and radial-velocity perturbations arising from non-sphericity and from phase-dependent variations in the shapes of the components.

For the present study, we add information from the out-of-eclipse variations in the light curve to model asynchronous rotation of the components and as a first step toward accounting for the presence of surface spots (§2.3.1). As part of our ongoing study of 2M0535–05, we plan to incorporate progressively more advanced treatments, including a full investigation of surface spots and inclusion of state-of-the-art brown-dwarf model atmospheres. Here, as in Paper I, we use simple blackbody spectra in our light curve models. While brown-dwarf spectra are known to exhibit strong departures from simple blackbodies, we show below that this effect is unlikely to significantly alter our principal findings; in particular, the reversal of temperatures with mass that we find in 2M0535–05 is probably not the result of improperly modeled spectra. On the other hand, understanding the temperature reversal may ultimately require a proper treatment of surface spots and their influence on the time- and aspect-dependent emergent flux from the system.

2.3.1. Spot-related variations in the light curve

To begin, we ran an initial WD fit to the light-curve and radial-velocity data (Tables 2 and 4) using as initial values the system’s orbital and physical parameters from Paper I, together with the updated orbital period from this study (§2.2). The best-fit parameters and their formal uncertainties are summarized in Table 5. The reduced χ^2 of this fit is large ($\chi_\nu^2 = 3.10$), and the r.m.s. of the residuals relative to this fit (0.033 mag) is accordingly larger than expected given the typical error on the photometric measurements (§2.2). This suggests an additional source of variability in the light curve—spots, for example—not included in the model.

Surface spots are most commonly manifested as low-amplitude, periodic, roughly sinusoidal variations superposed on the eclipse light curve (e.g. Stassun et al. 2004a). We searched for such low-amplitude, periodic variations in the light curve of 2M0535–05 by applying a Lomb-Scargle periodogram (Scargle 1982) analysis to those portions of the light-curve data obtained outside of eclipse. We performed this periodogram analysis separately on each epoch of light-curve data (see Table 3), as spot-related variations often show evolution in amplitude and phase with time (Stassun et al. 1999; Torres & Ribas 2002; Stassun et al. 2004a).

We find statistically significant periodic signals in all but the first two epochs, these earlier epochs possessing relatively few measurements. While the amplitudes of these periodic signals vary slightly from epoch to epoch, they are always small ($\Delta m \lesssim 0.06$ mag, peak-to-peak). Importantly, the periods of these signals are consistent across epochs, with a value of $P_{\text{spot}} \approx 3.3$ d. Spot-related variability observed in other eclipsing binaries is similarly characterized by photometric amplitudes of a few percent and periods that are constant over many epochs (e.g. Ribas 2003), most likely reflecting the rotation period of one or both binary components. The implication here is that at least one of the brown dwarfs in 2M0535–05 is nearly always

spotted, and rotates with $P_{\text{rot}} \approx 3.3$ d.

With a rotation period that is shorter than the orbital period by a factor of (almost exactly) 3, the rotational and orbital angular velocities of 2M0535–05 have evidently not yet become pseudo-synchronized with one another (where the rotational angular velocity is synchronized to the orbital angular velocity at periastron; Hut 1981), which for the eccentricity of 2M0535–05 would give $P_{\text{rot}}/P_{\text{orb}} \approx 1/2$. Instead, the rotation of at least one component in 2M0535–05 is super-synchronous. Such super-synchronicity is probably not surprising given the extreme youth of 2M0535–05 (see below) and that young brown dwarfs tend to be rapid rotators (Mohanty & Basri 2003); tidal effects have likely not yet had sufficient time to synchronize the system (e.g. Meibom & Mathieu 2005).

A more detailed discussion of rotation in 2M0535–05 is beyond the scope of this paper. For our present purposes, we proceed to adopt the observed $P_{\text{rot}} = 3.3$ d in our final WD fit as a constraint on the oblateness of both 2M0535–05 components. In addition, we rectify the I_C -band light curve by subtracting a sinusoid of $P = 3.3$ d, with the amplitude and phase determined separately for each epoch of data, as described above. The aim of this rectification procedure is to “remove” the spot signal from the light curve and to thereby allow the WD model to achieve goodness of fit without introducing additional spot-fitting parameters that are poorly constrained at present. We caution, however, that this procedure is *not* equivalent to modeling the spots physically. The inclusion of additional light curves at multiple wavelengths into our analyses (Gómez Maqueo Chew et al. 2007) will ultimately be required to constrain the physical properties of the spots and to permit full modeling of their effects on the observed light curves and radial velocities. Bearing these caveats in mind, we proceed with our analysis below using the rectified I_C -band light curve, and revisit the possible influence of spots in §3.2.

2.3.2. Determination of physical parameters

The final WD solution was determined by simultaneously fitting the *Phoenix* radial velocities and the I_C -band light curve, rectified as described above. The resulting orbital and physical parameters of 2M0535–05 are summarized in Table 5, the fit to the radial velocities shown in Fig. 2, the fit to the light curve displayed in Fig. 3, and the system geometry illustrated in Fig. 4. With the light curve rectified, the WD fit is now excellent; the r.m.s. of the residuals is 0.021 mag, comparable to the typical error on the photometric measurements (§2.2), and the goodness-of-fit is correspondingly very good, $\chi^2_{\nu} = 1.035$.

A comparison of the orbital and physical properties of 2M0535–05 derived from the rectified and unrectified light curves (Table 5) reveals mostly minor, statistically insignificant, differences in the fit parameters. However, a few parameters do show differences that are larger than their formal uncertainties. For example, both e and ω differ by $\sim 2\sigma$ (although these parameters are strongly correlated with one another, so their uncertainties are not independent), suggesting that the rectification procedure is not entirely free of small, systematic couplings to some parameters. Thus, while a physical treatment of spots in the WD model will ultimately be required to achieve full accuracy in the determination of some parameters, the effects of spots on the most fundamental physical parameters that we derive for 2M0535–05—the orbital parameters, in particular, and thus the component masses and radii—are probably insignificant. Moreover, if other parameters remain susceptible to spot-modeling effects, these effects are evidently very subtle.

We note that there exists an alternative WD solution to the one presented in Table 5, with nearly identical best-fit parameters except that the component radii are reversed. Formally, the goodness-of-fit of this alternative solution is inferior, with $\chi^2_{\nu} = 1.062$, but it is nonetheless acceptable. This particular type of degener-

acy is a general feature of eclipsing-binary solutions (see, e.g., Stassun et al. 2004a; López-Morales & Ribas 2005). Since only the component radii are significantly different in the two solutions, the degeneracy can be broken by adding the additional constraint of the luminosity ratio, which is generally very different in the two solutions. In this case, the preferred solution from Table 5 gives an H -band luminosity ratio of $L_1/L_2 = 1.63 \pm 0.13$, whereas the alternative solution gives $L_1/L_2 = 0.69 \pm 0.06$. The luminosity ratio predicted by the alternative solution—in which the secondary is both warmer and larger, and thus more luminous, than the primary—is clearly inconsistent with the ratio inferred from the observed spectra, which imply $L_1/L_2 \sim 1.5$ in the H band (see Fig. 1).

3. Results

3.1. Masses and Radii

With masses of $M_1 = 0.0569 \pm 0.0046 M_\odot$ and $M_2 = 0.0358 \pm 0.0028 M_\odot$, the components of 2M0535–05 are proven to be *bona fide* brown dwarfs. Moreover, with radii of $R_1 = 0.674 \pm 0.023 R_\odot$ and $R_2 = 0.485 \pm 0.018 R_\odot$, these brown dwarfs are more comparable in their physical dimensions to young, low-mass stars than to old brown dwarfs, consistent with their being very young (see below). Importantly, these mass and radius measurements are distance independent. Moreover, systematic errors do not appear to dominate over random measurement uncertainties (§2.1). Thus the masses and radii of 2M0535–05 reported here are accurate to 8% and 3%, respectively. In §3.4 we make use of these measurements for an initial examination of the predictions of theoretical brown-dwarf evolutionary models.

3.2. Reversal of temperatures

The physical properties that we have determined for the brown dwarfs in 2M0535–05 are surprising in at least one important respect: The less-massive secondary is hotter than the primary. Specifically, we find $T_{\text{eff},2}/T_{\text{eff},1} = 1.064 \pm 0.004$ (Table 5), which follows from the relative depths of the eclipses and bolometric corrections from the model atmospheres (blackbodies in this case), with small corrections for differences in occulted areas that occur due to the mildly eccentric orbit (Fig. 4). This finding is highly statistically significant. Such a reversal of temperatures with mass is not predicted by any theoretical model for coeval brown dwarfs—in which temperature increases monotonically with mass—and thus merits closer scrutiny. Here we consider the possible effects of non-blackbody atmospheres and surface spots.

Brown dwarf spectra deviate significantly from an ideal blackbody, due primarily to the strong wavelength dependence of molecular opacity. The corresponding redistribution of flux into or out of any specific wavelength depends on temperature, potentially affecting the ratio of eclipse depths. However, the primary and secondary of 2M0535–05 have very similar effective temperatures (§2.1), so both components should have similar deviations from a blackbody.

To check this quantitatively, we have examined up-to-date synthetic models of brown-dwarf spectra for temperatures appropriate to the components of 2M0535–05. In particular, we use the solar-metallicity COND¹ atmosphere models of Allard et al. (2001). As the masses and radii of 2M0535–05 imply $\log g \approx 3.5$

¹At the temperatures of the components of 2M0535–05, the DUSTY atmosphere models of these authors are very similar and would work equally well for our purposes. See also Mohanty & Basri (2003).

for both components, we use the COND models with this $\log g$ value also. The COND models incorporate recent opacities, including ~ 500 million molecular lines, as well as dust formation and condensation at very low temperatures. (For a more detailed discussion of these models, and their applicability to young brown dwarfs in particular, we point the reader to the extensive discussion in Mohanty & Basri (2003)). The results of our analysis are summarized in Fig. 5. We find that, while dramatic departures from simple blackbodies are clearly present in the model spectra, the ratio of surface brightnesses in the I band is consistent with that predicted from simple blackbodies to within 2%, which implies a T_{eff} ratio that is consistent with the blackbody value to within 0.5%.

As an additional check, we calculated the T_{eff} 's of the components of 2M0535–05 independently at 1.25, 1.65, and 2.2 μm . We use the ratio of surface fluxes at 0.8 μm (measured directly from the ratio of eclipse depths in the I_C -band light curve; §2.3) and the radii (measured directly from the eclipse durations and the orbital velocities; Table 5), together with an assumed distance to the Orion Nebula Cluster of 450 pc, empirical bolometric corrections from the literature (Golimowski et al. 2004), and the observed JHK magnitudes at these wavelengths from Carpenter et al. (2001): $K = 13.58 \pm 0.02$, $J - H = 0.640 \pm 0.015$, and $H - K = 0.385 \pm 0.015$. We derive temperatures of $T_1 = 2730$ K and $T_2 = 2875$ K (1.25 μm), $T_1 = 2675$ K and $T_2 = 2860$ K (1.65 μm), and $T_1 = 2680$ K and $T_2 = 2795$ K (2.2 μm). In all cases, the derived T_{eff} 's are consistent with a spectral type of $\sim\text{M6.5}$, and in all cases the reversal of temperatures persists.

Another potential contributor to non-blackbody spectra is the presence of hot or cold spots (akin to solar plage or sunspots) on the brown dwarfs, leading to spectra that derive from a combination of temperatures. Cool spots have now been found to be present on many brown dwarfs (e.g. Scholz & Eisloffel 2005) and may thus be expected on one or both brown dwarfs in 2M0535–05 as well. Indeed, we find a clear periodic signal in the out-of-eclipse portions of the I_C -band light curve, with a period of $P_{\text{spot}} \approx 3.3$ d and a semi-amplitude of ~ 0.03 mag (§2.3.1); almost certainly this is a rotationally modulated spot signal.

Such spot signals are commonly observed in the light curves of close eclipsing binaries, though modeling these effects is often a largely cosmetic exercise with little effect on the resulting stellar properties. For example, in our analysis of the young eclipsing binary V1174 Ori (Stassun et al. 2004a), we successfully reproduced the observed out-of-eclipse light-curve variations by including spots in the light-curve model, but the derived system parameters were altered only negligibly as a result (see also Torres & Ribas 2002; Ribas 2003; López-Morales & Ribas 2005).

On the other hand, accurate modeling of spot effects can be crucially important for the proper interpretation of certain systems. W UMa stars of the so-called “W type” are a particularly good case in point. A defining characteristic of these systems is that the deeper eclipse corresponds to the occultation of the physically smaller and lower-mass secondary, similar to what is observed in 2M0535–05. One interpretation advanced early on by Rucinski (1974) is that the secondary is hotter than the primary (typically by $\sim 5\%$), perhaps due to thermal effects arising from mass- and energy-transfer in these contact systems. However, an alternate interpretation (e.g. Eaton et al. 1980) is that cool spots on the primary, if preferentially located along the eclipsed latitude and more-or-less uniformly distributed in longitude, can have the effect of lowering the surface brightness of the eclipsed regions on the primary during transit by the secondary, thus making the eclipse of the primary shallower. Such a model is generally very delicate in the details, and requires careful arrangement of the putative spots in order that they produce only mild ($\lesssim 0.05$ mag) out-of-eclipse variations in the light curve; the inferred spot configurations can resemble a “leopard print” pattern in some cases (e.g. Linnell 1991).

We are now experimenting with more sophisticated light-curve models that include the effects of spots.

In the meantime, we emphasize here that the ratio of eclipsed surface brightnesses implied by our current light-curve model is robust; the higher-mass primary really does radiate less per unit area than the secondary, at least at those surface elements that are eclipsed by the secondary. Thus, in what follows, we continue to explore the implications of a temperature reversal in 2M0535–05.

3.3. Physical association with the Orion Nebula star-forming region: Evidence for youth

Strong evidence for the physical association of 2M0535–05 with the Orion Nebula Cluster, and hence of its youth, is provided by its center-of-mass velocity. The observed value of $\gamma = 24.1 \pm 0.4 \text{ km s}^{-1}$ (Table 5) is within 1 km s^{-1} of the systemic radial velocity ($25 \pm 1.5 \text{ km s}^{-1}$) of kinematic members of this active star-forming region (Stassun et al. 1999; Sicilia-Aguilar et al. 2005).

In addition, we can derive a distance to 2M0535–05 by comparing the total system luminosity to its observed flux. To calculate the luminosity, we use the directly measured radii (Table 5) together with the effective temperatures and apply the Stefan-Boltzmann relation, $L = 4\pi R^2 \sigma_B T_{\text{eff}}^4$. The adopted spectral type of $M6.5 \pm 0.5$ for the 2M0535–05 primary (§2.1) implies $T_{\text{eff},1} = 2715 \pm 100 \text{ K}$ based on recent calibrations of the T_{eff} scale for brown dwarfs (Mohanty & Basri 2003; Slesnick et al. 2004; Golimowski et al. 2004), though as mentioned earlier, systematic uncertainties in the T_{eff} scale may be as large as $\sim 200 \text{ K}$. From the measured temperature ratio of $T_{\text{eff},2}/T_{\text{eff},1} = 1.064 \pm 0.004$ (Table 5), we obtain $T_{\text{eff},2} = 2820 \pm 105 \text{ K}$. This then gives component luminosities of $L_1 = 0.0223 \pm 0.0034 L_{\odot}$ and $L_2 = 0.0148 \pm 0.0023 L_{\odot}$, and a total system luminosity of $L = 0.0372 \pm 0.0060 L_{\odot}$. Adopting an apparent magnitude of $m_K = 13.58 \pm 0.02$ (Carpenter et al. 2001) and bolometric corrections appropriate for the observed T_{eff} 's (Golimowski et al. 2004) yields a derived distance to 2M0535–05 of $456 \pm 34 \text{ pc}$, assuming no extinction. This distance determination is consistent with the distance to the Orion Nebula of $480 \pm 80 \text{ pc}$ (Genzel & Stutzki 1989).

The Orion Nebula Cluster is extremely young, with an age that has been estimated to be just 1_{-1}^{+2} Myr (Palla & Stahler 1999; Hillenbrand 1997). With a center-of-mass velocity and distance that are both consistent with membership in this cluster, 2M0535–05 is probably also very young, likely having formed within the past few Myr. In addition, as discussed in Paper I, the JHK colors of 2M0535–05 place an upper limit on the extinction of $A_V < 0.75$, and thus limit the amount of remnant material available to the brown dwarfs for ongoing accretion. Given the eclipsing nature of the system, any disk material would necessarily be seen edge-on and would thus produce a large amount of extinction and reddening. Thus, while the colors of 2M0535–05 are formally consistent with a small amount of interstellar extinction and/or a small amount of remnant disk material, the currently observed masses are unlikely to change significantly over time. These brown dwarfs will likely forever remain brown dwarfs.

3.4. Comparison to theoretical brown-dwarf evolutionary tracks

While we expect that our ongoing analysis of 2M0535–05 will further improve the accuracy of the measured system parameters, the present accuracy is sufficient to permit an initial examination of theoretical brown-dwarf evolutionary models. Here we consider two of the more widely used sets of tracks: those of Baraffe et al. (1998)² and those of D'Antona & Mazzitelli (1997, updated 1998). These models differ in

²We use the tracks with convection mixing-length parameter $\alpha = 1.0$, as recent analyses of young, low-mass stars and brown dwarfs suggest that such low-efficiency convection best matches the observed physical properties of these objects (e.g.

their treatment of brown-dwarf atmospheres and of energy transport (convection) in brown-dwarf interiors, as well as in the choice of initial conditions (for a more in-depth discussion of differences in these models, see Siess et al. 2000; Baraffe et al. 2002).

Fig. 6 compares the observed radii, effective temperatures, and luminosities of 2M0535–05 with the values theoretically predicted by these models for brown dwarfs with masses of $M_1 = 0.0569 \pm 0.0046 M_\odot$ and $M_2 = 0.0358 \pm 0.0028 M_\odot$ (Table 5).

We note first that, generally speaking, the agreement between the observed and theoretically predicted properties of 2M0535–05 is quite good. The models predict that these very young brown dwarfs should, at an age of ~ 1 Myr, be significantly larger, warmer, and more luminous than their older counterparts—and that is in fact what we see. Indeed, between 1 and 100 Myr, a brown dwarf with a mass of $0.057 M_\odot$ (the mass of the 2M0535–05 primary) is predicted to shrink by 500%, cool by several hundred K (or, equivalently, go from an M spectral class to an L spectral class), and dim by 1.5 orders of magnitude (Fig. 6). The recently measured radius ($R = 0.12 R_\odot$) of the old and low-mass ($M = 0.09 M_\odot$) star in the eclipsing binary system OGLE-TR-122 (Pont et al. 2005) confirms that stars with near-brown-dwarf masses have very small radii ($\sim 1 R_{\text{Jup}}$) when they are old. Thus, the fact that 2M0535–05 comprises young brown dwarfs that are both large and luminous—and even simply that they are of M spectral class, as predicted—is a testament to the generally good predictive power of current theoretical models of brown dwarfs.

At a more detailed level, the models of D’Antona & Mazzitelli (1997) predict radii and luminosities that are more consistent with the observed values. The difference is most pronounced in the radii; the Baraffe et al. (1998) models under-predict both radii by $\sim 10\%$. This finding of under-predicted model radii is similar in sense and magnitude to that found from recent efforts to derive the physical properties of low-mass stars and brown dwarfs through detailed modeling of their spectra (Mohanty et al. 2004a,b). In addition, while both sets of models perform reasonably well with respect to the observed luminosities, the agreement is somewhat better for the D’Antona & Mazzitelli (1997) models; it appears possible that more accurate measurements will reveal an under-prediction of luminosity by the Baraffe et al. (1998) models for the lower-mass secondary.

But perhaps more importantly, the reversal of temperatures in 2M0535–05 remains puzzling; the relationship between effective temperature and mass is predicted by both sets of models to be monotonic for brown dwarfs of the same age. However, this expectation disappears for two brown dwarfs of differing age. The observed effective temperatures can be seen as consistent with the D’Antona & Mazzitelli (1997) models if the primary is taken as being modestly younger than the secondary ($\Delta\tau \approx 0.5$ Myr). Indeed, the temperatures, radii, and luminosities of 2M0535–05 all remain in marginally good agreement with these models for such an age difference, at a mean age of 1 Myr (Fig. 7), if we also adjust the observed T_{eff} scale cooler by 70 K. Such a shift is well within the current systematic uncertainty of the brown-dwarf T_{eff} scale (§2.1). Thus, a question raised by our findings is whether current brown-dwarf formation theory can accommodate a scenario in which two brown dwarfs—that are part of the same, very young, binary system—can have sufficiently different ages to allow for reversed temperatures as we have observed in 2M0535–05.

Stassun et al. 2004a; Mathieu et al. 2006; Torres et al. 2006).

4. Discussion

4.1. 2M0535–05 as a case study in dynamical brown-dwarf formation?

In truth, we have very little understanding about how binaries with components as close as those in 2M0535–05 are formed (see, e.g., Bonnell 2001; Tohline 2002). (2M0535–05 is, after PP1 15 in the Pleiades (Basri & Martín 1999), the shortest-period brown-dwarf binary system yet discovered). With a few exceptions (e.g. Tohline & Durisen 2001), fission seems to be ruled out. *In situ* mechanisms involving dynamic cloud fragmentation and disk fragmentation have not yet proven successful in creating such close binaries, but remain to be fully developed. In particular, the role of orbital migration in the presence of a massive circumbinary disk needs to be considered. Certainly, if the two brown dwarfs formed together as a close binary, we have essentially no *a priori* expectations for whether they should be observed to be coeval to within 0.5 Myr.

Alternatively, recent theoretical work (Reipurth & Clarke 2001), as well as detailed numerical simulations (Bate et al. 2002a,b; Bate & Bonnell 2005), suggest that dynamical interactions may be integral to the formation of brown dwarfs. The argument is essentially that strong gravitational interactions in multiple-body encounters provide a feasible mechanism for disrupting the accretion process, and thereby preventing the accumulation of mass by objects that would otherwise have become stars. This hypothesis remains under debate (e.g. Maxted & Jeffries 2005). Still, it is tempting to speculate that the components of 2M0535–05 did not form together as a binary, but rather formed separately—with the primary forming later—and then were later married through a dynamical interaction. In such a scenario, it is possible that the resulting binary system—comprising two objects that were not originally formed together—may exhibit seemingly peculiar characteristics, such as the observed reversal of effective temperatures, that in fact reveal the non-coeval nature of the system.

There are at least two specific scenarios involving multiple-body interactions that might pertain to the origin of 2M0535–05. One involves a low-mass binary pair that interacts with a more massive third body from elsewhere in the cluster. Simulations show that, if the binary is not simply broken apart by the encounter, the lower-mass member of the binary is ejected and replaced by the massive incoming object (Bate et al. 2002a). The resulting binary would then likely consist of non-coeval members. A serious concern with this scenario in the context of 2M0535–05 is that it is unlikely in three-body encounters within clusters that the most massive object would have a mass of only $0.06 M_{\odot}$.

Thus, a second scenario is that several objects formed in the fragmentation of a small molecular core, forming an unstable multiple system. The consequent rapid dynamical evolution of the system may have both terminated accretion and formed a hard binary (Bate et al. 2002b). In such a fragmentation scenario the relative core-collapse times and evolutionary zero points might easily vary by 0.5 Myr, of order the age difference needed to explain the temperature reversal of 2M0535–05 in the context of some evolutionary models (Fig. 7).

The position of 2M0535–05 might be taken as further evidence that dynamics have been important in its history. With a projected separation of 2.8 pc from the center of the Orion Nebula, 2M0535–05 is situated more than 10 core radii from the center of the Orion Nebula Cluster (Hillenbrand & Hartmann 1998); perhaps the pair was ejected from the cluster center during a dynamical encounter. The one-dimensional velocity dispersion in the cluster is $\sim 2 \text{ km s}^{-1}$ (van Altena et al. 1988; Hillenbrand & Hartmann 1998; Stassun et al. 1999; Sicilia-Aguilar et al. 2005), so to reach its current position in 1 Myr, if ejected from the cluster core, 2M0535–05 would need a somewhat higher-than-usual velocity of $\sim 3 \text{ km s}^{-1}$ in the plane of

the sky. However, the measured center-of-mass radial velocity of 2M0535–05 does not deviate significantly from the cluster velocity. An alternative interpretation for the position of 2M0535–05 at the outskirts of the cluster may be that it is not a member of the Cluster proper, but rather a member of the more widely distributed population of young stars in the region surrounding the Orion Nebula (Warren & Hesser 1978). The binary’s proper motion is the critical measurement needed to establish whether 2M0535–05 was ejected from the cluster center.

4.2. Missing physics in theoretical brown-dwarf evolutionary tracks?

An alternative explanation is that the evolutionary tracks are deficient with respect to some critical physical ingredient(s). For example, the presence of strong magnetic fields on one or both brown dwarfs in 2M0535–05 could be affecting energy transport and thereby altering their physical structure.

Indeed, recent analyses of several young, low-mass eclipsing binaries (e.g. Stassun et al. 2004a; Covino et al. 2004; Torres et al. 2006) indicate systematic discrepancies in the models. In particular, the observed effective temperatures are cooler than expected, and the observed radii larger than expected. These discrepancies are especially pronounced among the most magnetically active stars (as traced by X-ray emission and other proxies). One possible interpretation is that strong magnetic fields inhibit energy transport in these otherwise fully convective stars, resulting in a decrease of the surface temperature and a corresponding increase in radius so as to radiate the same total flux (Montalbán & D’Antona 2006). Such an interpretation would be consistent with, and would help explain, the emerging observational evidence for suppressed convection in young, low-mass stars (e.g. Stassun et al. 2004a; Mathieu et al. 2006; Torres et al. 2006, and references therein).

In this context, the temperature reversal in 2M0535–05 might be taken as evidence for a strong magnetic field on the higher-mass primary that is causing a sufficient decrease in its surface temperature to make it effectively cooler than the lower-mass secondary. By inference, the secondary would be interpreted as being less magnetically active. The observational evidence is strong for magnetic activity in young, low-mass stars and brown dwarfs of early- and mid-M type (e.g. Mohanty et al. 2002; Stassun et al. 2004; Preibisch et al. 2005). Moreover, the evidence in fact shows a marked decline in magnetic activity at very late M types (e.g. Gizis et al. 2000; Mohanty et al. 2002), suggesting that brown dwarfs with roughly the mass of the 2M0535–05 secondary and below are not capable of generating strong fields. The idea of a magnetically active primary would also be consistent with the primary being heavily spotted (see §3.2).

If we are to explain the anomalously low effective temperature of the 2M0535–05 primary in this way, we should then also expect its radius to be larger than theoretically predicted, as the one effect goes hand in hand with the other (Montalbán & D’Antona 2006). As discussed above (§3.4), whether the 2M0535–05 radii agree with theoretical predictions depends on one’s choice of model. The Baraffe et al. (1998) tracks do indeed suggest over-sized radii in 2M0535–05 (for *both* components), though this may simply reflect the truncation of those tracks at 1 Myr. On the other hand, the D’Antona & Mazzitelli (1997) tracks agree with the observed radii very well (Fig. 6), with no need to invoke missing physics.

5. Summary and Conclusions

2M0535–05 is the first known eclipsing binary system comprising two brown dwarfs. Satisfying both kinematic and distance requirements for physical association with the young (~ 1 Myr) Orion Nebula Cluster, 2M0535–05 provides the only direct, accurate measurements of the fundamental physical properties of newly formed sub-stellar objects. The masses that we measure are accurate to $\sim 10\%$, the radii accurate to $\sim 5\%$, the ratio of effective temperatures accurate to $\sim 1\%$, and all are distance independent. As such, 2M0535–05 represents an important benchmark for theoretical models of brown-dwarf formation and evolution.

Encouragingly, we find that current brown-dwarf evolutionary tracks are, broadly speaking, successful in predicting the fundamental physical properties of these young brown dwarfs. More quantitatively, of the two sets of theoretical models considered here, we find that the models of D’Antona & Mazzitelli (1997) yield mass-radius and mass-luminosity relationships that best agree with the empirically determined ones. The models of Baraffe et al. (1998) predict radii and luminosities that are $1.5\text{--}2\sigma$ smaller than the observed values.

However, the reversal of component effective temperatures with mass in 2M0535–05 is unexpected and unexplained. We have considered here two possible interpretations of this intriguing result. The first is that the components of 2M0535–05 are mildly non-coeval, with the higher-mass primary being ~ 0.5 Myr younger than the secondary. The models of D’Antona & Mazzitelli (1997) are in fact consistent with the observed temperature reversal for such an age difference. A second hypothesis is that strong magnetic activity on the primary is inhibiting convection, and thereby lowering its surface temperature.

Neither of these interpretations is wholly satisfying, and neither is obviously discreditable. Binary formation theory is largely silent on the subject of coevality at the level of ~ 0.5 Myr, and theorists have long warned the star-formation community about the limited applicability of evolutionary track chronometry at such early ages (the model zero-points being arbitrary in most cases). In addition, while the observational evidence is strong that young brown dwarfs can be magnetically active, the effects of magnetic fields on brown-dwarf structure and evolution have yet to be consistently modeled or fully understood.

This research is supported by NSF grant AST-0349075, and by a Cottrell Scholar award from the Research Corporation, to K.G.S., and by NSF grant AST-9731302 to R.D.M. This work is based in part on observations obtained through queue program GS-2002B-Q-11 at the Gemini Observatory, which is operated by the Association of Universities for Research in Astronomy, Inc., under a cooperative agreement with the NSF on behalf of the Gemini partnership: the National Science Foundation (United States), the Particle Physics and Astronomy Research Council (United Kingdom), the National Research Council (Canada), CONICYT (Chile), the Australian Research Council (Australia), CNPq (Brazil) and CONICET (Argentina). The WIYN Observatory is a joint facility of the University of Wisconsin–Madison, Indiana University, Yale University, and the National Optical Astronomy Observatories.

REFERENCES

- Allard, F., Hauschildt, P. H., Alexander, D. R., Tamanai, A., & Schweitzer, A. 2001, *ApJ*, 556, 357
- Andersen, J. 1991, *A&A Rev.*, 3, 91
- Baraffe, I., Chabrier, G., Allard, F., & Hauschildt, P. H. 1998, *A&A*, 337, 403

- Baraffe, I., Chabrier, G., Allard, F., & Hauschildt, P. H. 2002, *A&A*, 382, 563
- Basri, G. 2000, *ARA&A*, 38, 485
- Basri, G., & Martín, E. L. 1999, *AJ*, 118, 2460
- Bate, M. R., & Bonnell, I. A. 2005, *MNRAS*, 356, 1201
- Bate, M. R., Bonnell, I. A., & Bromm, V. 2002a, *MNRAS*, 332, L65
- Bate, M. R., Bonnell, I. A., & Bromm, V. 2002b, *MNRAS*, 336, 705
- Bayless, A. J., & Orosz, J. A. 2006, *ApJ*, 651, 1155
- Bender, C., Simon, M., Prato, L., Mazeh, T., & Zucker, S. 2005, *AJ*, 129, 402
- Bonnell, I. A. 2001, *IAU Symposium*, 200, 23
- Burrows, A., Hubbard, W. B., Lunine, J. I., & Liebert, J. 2001, *Reviews of Modern Physics*, 73, 719
- Carpenter, J. M., Hillenbrand, L. A., & Skrutskie, M. F. 2001, *AJ*, 121, 3160
- Carpenter, J. M. 2001, *AJ*, 121, 2851
- Chabrier, G., & Baraffe, I. 2000, *ARA&A*, 38, 337
- Covino, E., Frasca, A., Alcalá, J. M., Paladino, R., & Sterzik, M. F. 2004, *A&A*, 427, 637
- D’Antona, F., & Mazzitelli, I. 1997, *Memorie della Societa Astronomica Italiana*, 68, 807
- Eaton, J. A., Wu, C.-C., & Rucinski, S. M. 1980, *ApJ*, 239, 919
- Genzel, R., & Stutzki, J. 1989, *ARA&A*, 27, 41
- Gizis, J. E., Monet, D. G., Reid, I. N., Kirkpatrick, J. D., Liebert, J., & Williams, R. J. 2000, *AJ*, 120, 1085
- Golimowski, D. A., et al. 2004, *AJ*, 127, 3516
- Gómez Maqueo Chew, Y., Stassun, K. G., Vaz, L. P. R., & Mathieu, R. D. 2007, in preparation
- Hillenbrand, L. A., & Hartmann, L. W. 1998, *ApJ*, 492, 540
- Hillenbrand, L. A. 1997, *AJ*, 113, 1733
- Hinkle, K., Wallace, L., & Livingston, W. 1995, *PASP*, 107, 1042
- Hut, P. 1981, *A&A*, 99, 126
- Kallrath, J., & Milone, E. F. 1999, *Eclipsing binary stars : modeling and analysis / Joseph Kallrath, Eugene F. Milone. New York : Springer, 1999. (Astronomy and astrophysics library)*
- Linnell, A. P. 1991, *ApJ*, 383, 330
- Linnell, A. P. 1987, *ApJ*, 316, 389
- López-Morales, M., & Ribas, I. 2005, *ApJ*, 631, 1120

- Mathieu, R. D., Baraffe, I., Simon, M., Stassun, K.G., & White, R. 2006, *Protostars and Planets V*, in press
- Maxted, P. F. L., & Jeffries, R. D. 2005, *MNRAS*, 362, L45
- Mazeh, T., Prato, L., Simon, M., Goldberg, E., Norman, D., & Zucker, S. 2002, *ApJ*, 564, 1007
- Meibom, S., & Mathieu, R. D. 2005, *ApJ*, 620, 970
- Mohanty, S., Jayawardhana, R., & Basri, G. 2004, *ApJ*, 609, 885
- Mohanty, S., Basri, G., Jayawardhana, R., Allard, F., Hauschildt, P., & Ardila, D. 2004, *ApJ*, 609, 854
- Mohanty, S., & Basri, G. 2003, *ApJ*, 583, 451
- Mohanty, S., Basri, G., Shu, F., Allard, F., & Chabrier, G. 2002, *ApJ*, 571, 469
- Montalbán, J., & D’Antona, F. 2006, *MNRAS*, 713
- Nakajima, T., Oppenheimer, B. R., Kulkarni, S. R., Golimowski, D. A., Matthews, K., & Durrance, S. T. 1995, *Nature*, 378, 463
- Neuhäuser, R., et al. 1998, *A&A*, 334, 873
- Palla, F., & Stahler, S. W. 1999, *ApJ*, 525, 772
- Pont, F., Melo, C. H. F., Bouchy, F., Udry, S., Queloz, D., Mayor, M., & Santos, N. C. 2005, *A&A*, 433, L21
- Prato, L., Simon, M., Mazeh, T., McLean, I. S., Norman, D., & Zucker, S. 2002, *ApJ*, 569, 863
- Preibisch, T., et al. 2005, *ApJS*, 160, 401
- Prša, A., & Zwitter, T. 2005, *ApJ*, 628, 426
- Rebolo, R., Zapatero-Osorio, M. R., & Martin, E. L. 1995, *Nature*, 377, 129
- Reipurth, B., & Clarke, C. 2001, *AJ*, 122, 432
- Ribas, I. 2003, *A&A*, 398, 239
- Rucinski, S. 1999, *ASP Conf. Ser.* 185: *IAU Colloq. 170: Precise Stellar Radial Velocities*, 185, 82
- Rucinski, S. M. 1974, *Acta Astronomica*, 24, 119
- Scargle, J. D. 1982, *ApJ*, 263, 835
- Scholz, A., & Eislöffel, J. 2005, *A&A*, 429, 1007
- Sicilia-Aguilar, A., et al. 2005, *AJ*, 129, 363
- Siess, L., Dufour, E., & Forestini, M. 2000, *A&A*, 358, 593
- Slesnick, C. L., Hillenbrand, L. A., & Carpenter, J. M. 2004, *ApJ*, 610, 1045
- Stassun, K. G., Mathieu, R. D., & Valenti, J. A. 2006, *Nature*, 440, 311 (Paper I)
- Stassun, K. G., Mathieu, R. D., Vaz, L. P. R., Stroud, N., & Vrba, F. J. 2004a, *ApJS*, 151, 357

- Stassun, K. G., Ardila, D. R., Barsony, M., Basri, G., & Mathieu, R. D. 2004b, *AJ*, 127, 3537
- Stassun, K. G., Mathieu, R. D., Mazeh, T., & Vrba, F. J. 1999, *AJ*, 117, 2941
- Stellingwerf, R. F. 1978, *ApJ*, 224, 953
- Tohline, J. E. 2002, *ARA&A*, 40, 349
- Tohline, J. E., & Durisen, R. H. 2001, *IAU Symposium*, 200, 40
- Torres, G., Lacy, C. H., Marschall, L. A., Sheets, H. A., & Mader, J. A. 2006, *ApJ*, 640, 1018
- Torres, G., & Ribas, I. 2002, *ApJ*, 567, 1140
- Udry, S., Mayor, M., & Queloz, D. 1999, *ASP Conf. Ser.* 185: *IAU Colloq. 170: Precise Stellar Radial Velocities*, 185, 367
- van Altena, W. F., Lee, J. T., Lee, J.-F., Lu, P. K., & Upgren, A. R. 1988, *AJ*, 95, 1744
- Warren, W. H., Jr., & Hesser, J. E. 1978, *ApJS*, 36, 497
- Wilson, R. E., & Devinney, E. J. 1971, *ApJ*, 166, 605

Table 1. Standard stars

Name	SpTy	Exp. time (s)	Ref.
GJ 328	M0	180	Mazeh et al. (2002)
GJ 382	M1.5	180	Mazeh et al. (2002)
GJ 447	M4	120	Mohanty & Basri (2003)
GJ 406	M6	120	Mohanty & Basri (2003)
LHS 292	M6.5	3600	Mazeh et al. (2002)
LHS 3003	M7	900	Mohanty & Basri (2003)
GJ 3655	M8	3600	Mohanty & Basri (2003)
BRIB 1507–0229	M9	3600	Mohanty & Basri (2003)

Table 2. Radial velocity measurements of 2M0535–05

HJD ^a	Phase ^b	R.V. ^c km s ⁻¹	σ_{RV} km s ⁻¹	$(O - C)$ ^d km s ⁻¹
Primary				
2452623.74805	0.75
2452624.75701	0.85	9.59	1.41	1.34
2452625.72555	0.95	2.00	2.22	1.32
2452626.65154	0.04	9.84	1.75	-2.79
2452649.72938	0.40	38.02	1.41	1.30
2452650.67281	0.50	34.21	1.14	0.31
2452655.74512	0.02	6.61	2.56	-0.98
2452656.70824	0.12	25.58	1.28	-0.84
2453432.57920	0.45	37.09	2.11	1.62
$\chi^2_\nu = 0.7$				
Secondary				
2452623.74805	0.75	29.69	1.17	-2.50
2452624.75701	0.85	48.53	1.73	-0.41
2452625.72555	0.95	61.35	2.07	0.40
2452626.65154	0.04	42.43	2.97	0.43
2452649.72938	0.40	4.18	1.24	0.37
2452650.67281	0.50	5.07	2.00	-3.21
2452655.74512	0.02	50.04	2.35	0.05
2452656.70824	0.12	22.58	1.31	2.45
2453432.57920	0.45	6.64	2.64	0.85
$\chi^2_\nu = 1.2$				

^aHeliocentric Julian Date.

^bOrbital phase, relative to ephemeris of Table 5.

^cHeliocentric radial velocity.

^dResidual relative to WD solution (see text).

Table 3. Summary of I_C -band time-series photometry

Obs.	Telescope	HJD range ^a	N_{obs} ^b
1	KPNO 0.9-m	49699.70 – 49703.93	40
2	WISE 1.0-m	49698.35 – 49714.42	47
3	WIYN 0.9-m	52227.78 – 52238.01	102
4	WIYN 0.9-m	52595.75 – 52624.95	144
5	SMARTS 0.9-m	52622.57 – 52631.51	122
6	SMARTS 1.3-m	52922.73 – 53081.57	347
7	SMARTS 0.9-m	53011.57 – 53024.77	205
8	SMARTS 1.3-m	53280.74 – 53340.73	230
9	SMARTS 1.0-m	53373.56 – 53386.79	184
10	SMARTS 1.3-m	53403.53 – 53445.60	338
11	SMARTS 1.3-m	53646.82 – 53727.69	204
12	SMARTS 1.0-m	53719.59 – 53727.83	190
13	SMARTS 1.3-m	53745.64 – 53846.48	251

^aRange of Heliocentric Julian Dates (2400000+).

^bNumber of observations.

Table 4. Differential I_C -band light curve of 2M0535–05

HJD ^a	Δm^b	σ_m	Obs. ^c
2453686.70525	0.006	0.020	11
2453686.71293	0.016	0.054	11
2453687.76841	–0.004	0.052	11
2453687.77617	–0.006	0.052	11
2453687.78389	0.020	0.029	11
2453687.79158	–0.002	0.029	11
2453688.73523	–0.001	0.020	11
2453688.74295	–0.008	0.061	11
2453688.75066	0.022	0.020	11
2453688.75835	0.030	0.020	11
2453689.77018	0.262	0.025	11
2453689.77783	0.220	0.020	11
2453689.79309	0.237	0.062	11
2453690.71340	0.008	0.020	11

^aHeliocentric Julian Date

^bDifferential I_C magnitude (arbitrary zero-point).

^cSource of measurement (see Table 3).

Note. — The full table is available in the electronic version of the Journal. A portion is shown here for guidance regarding its form and content.

Table 5. Orbital and physical parameters of 2M0535–05

	Paper I	This study	
		Unrectified ^a	Rectified ^a
Orbital period, P [d]	9.779621 ± 0.000042	9.779556 ± 0.000019^b	
Time of periastron (Bessellian year), T_0	2001.863650 ± 0.000095	2001.863903 ± 0.000160	2001.863765 ± 0.000071
Eccentricity, e	0.3225 ± 0.0060	0.3354 ± 0.0049	0.3276 ± 0.0033
Orientation of periastron, ω [°]	215.4 ± 1.1	219.2 ± 1.4	217.0 ± 0.9
Semi-major axis, $a \sin i$ [A.U.]	0.0398 ± 0.0010	0.0406 ± 0.0016	0.0406 ± 0.0010
Center-of-mass velocity, γ [km s ⁻¹]	24.1 ± 0.4	24.1 ± 0.4	24.1 ± 0.4
Mass ratio, $q \equiv M_2/M_1$	0.625 ± 0.018	0.622 ± 0.022	0.631 ± 0.015
Total mass, $(M_1 + M_2) \sin^3 i$ [M _⊙]	0.0880 ± 0.0076	0.0932 ± 0.0111	0.0932 ± 0.0073
Inclination, i [°]	88.8 ± 0.2	89.4 ± 0.3	89.2 ± 0.2
Primary semi-amplitude, K_1 [km s ⁻¹]	...	18.37 ± 1.01	18.49 ± 0.67
Secondary semi-amplitude, K_2 [km s ⁻¹]	...	29.55 ± 1.24	29.30 ± 0.81
Primary mass, M_1 [M _⊙]	0.0541 ± 0.0046	0.0575 ± 0.0069	0.0572 ± 0.0045
Secondary mass, M_2 [M _⊙]	0.0340 ± 0.0027	0.0358 ± 0.0043	0.0360 ± 0.0028
Primary radius, R_1 [R _⊙]	0.669 ± 0.034	0.673 ± 0.037	0.675 ± 0.023
Secondary radius, R_2 [R _⊙]	0.511 ± 0.026	0.485 ± 0.029	0.486 ± 0.018
Primary gravity, $\log g_1$...	3.62 ± 0.14	3.62 ± 0.10
Secondary gravity, $\log g_2$...	3.54 ± 0.14	3.54 ± 0.09
Effective temperature ratio, T_2/T_1	1.054 ± 0.006	1.062 ± 0.006	1.064 ± 0.004

^aWD solutions based on fits to the unrectified and rectified I_C -band light curve (see §2.3).

^bUncertainty in the period is from a phase dispersion minimization (Stellingwerf 1978) analysis on the I_C -band light curve (see §2.2); the period is held fixed in the WD fit and its uncertainty propagated into the uncertainties of derived quantities.

Fig. 1.— Determination of the radial velocities of the primary and secondary components of 2M0535–05 using the Broadening Function (BF) analysis of Rucinski (1999). The example BF shown here (solid line) is from the spectrum of HJD 2452649 (see Table 2), where the primary and secondary are at near maximum velocity separation. An M6.5 dwarf was used as the radial-velocity template (see §2.1). The dashed line shows a two-gaussian fit to the BF, from which velocity centroids and their formal uncertainties are determined. The ratio of the peak areas from this fit is 1.6, indicating that the primary dominates the light of the system, contributing $\sim 60\%$ more flux than the secondary at the wavelength of these observations ($1.555 \mu\text{m}$).

Fig. 2.— Radial velocity measurements of 2M0535–05. The individual radial velocity measurements from Table 2 are plotted (primary measurements in green, secondary measurements in red), folded on the orbital period and phased to the time of periastron (see Table 5). The solid lines are WD models based on a simultaneous fit to the radial velocity measurements and the rectified I_C -band light curve (see Table 4 and Fig. 3). Distortions in the model curves near phases 0.075 and 0.75 are due to the brief occultations of the approaching and receding limbs of each component when it is eclipsed. Residuals are shown at bottom. Note: This figure appears in color in the electronic version of the journal.

Fig. 3.— I_C -band light curve of 2M0535–05. The individual photometric measurements from Table 4 are plotted, rectified using sinusoidal fits to the out-of-eclipse portions of the light curve (see §2.3), folded on the orbital period and phased to the time of periastron (see Table 5). The solid line is a WD model based on a simultaneous fit to the rectified I_C -band light curve and the *Phoenix* radial velocities (see Table 2). Residuals are shown at bottom. Insets show detail around primary and secondary eclipses, which in this system correspond to the eclipses of the secondary and primary components, respectively. The r.m.s. residual is 0.02 mag, comparable to the mean photometric error. The reduced χ^2 of the fit is 1.035. Note: this figure appears in color in the electronic version of the journal.

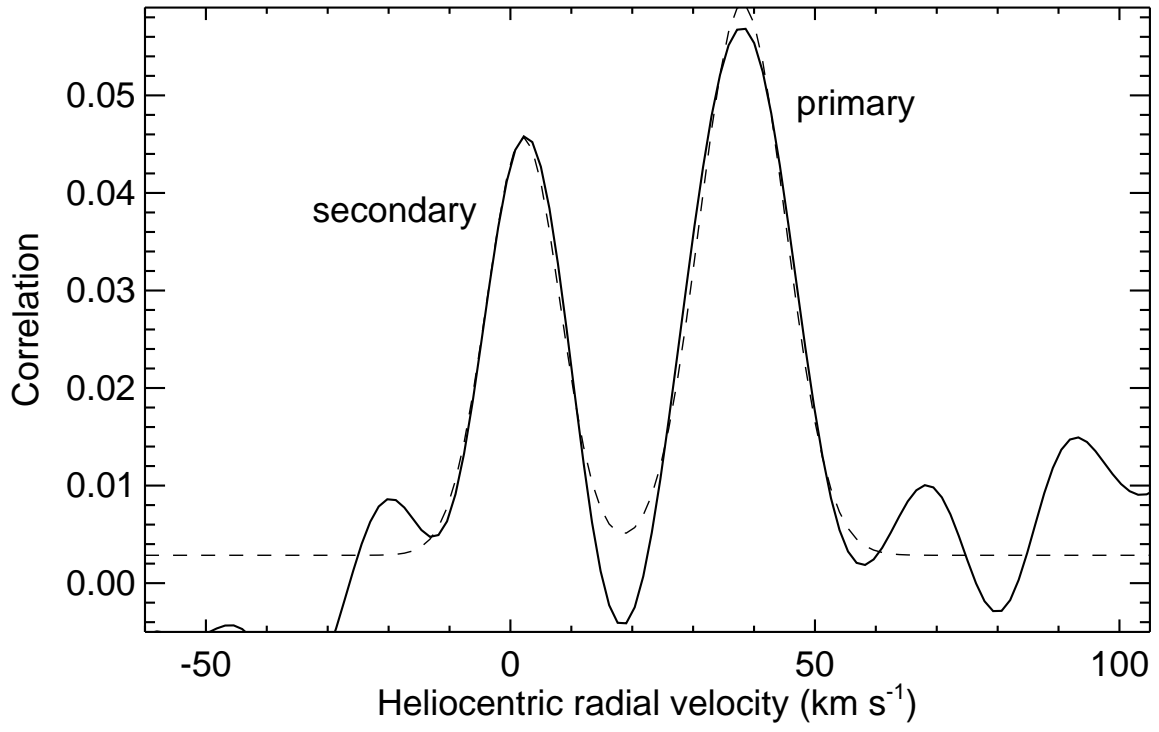
Fig. 4.— The geometry of the orbital plane of 2M0535–05 in the rest frame of the primary (more massive) brown dwarf is illustrated, to scale, at primary eclipse (orbital phase 0.075; see Fig. 3). The brown dwarfs are represented by filled circles, their radii also to scale (the adopted rotation period of $P_{\text{rot}} = 3.3 \text{ d}$ constrains the oblateness of both components to be less than 0.5%). The position of periastron (orbital phase 0.0) is indicated by a star symbol, and small arrows indicate the direction of the secondary’s orbit about the primary. The observer is to the left, as indicated by the arrow. Note that, at this orbital phase corresponding to the deeper eclipse, the secondary (less massive) brown dwarf is the one eclipsed.

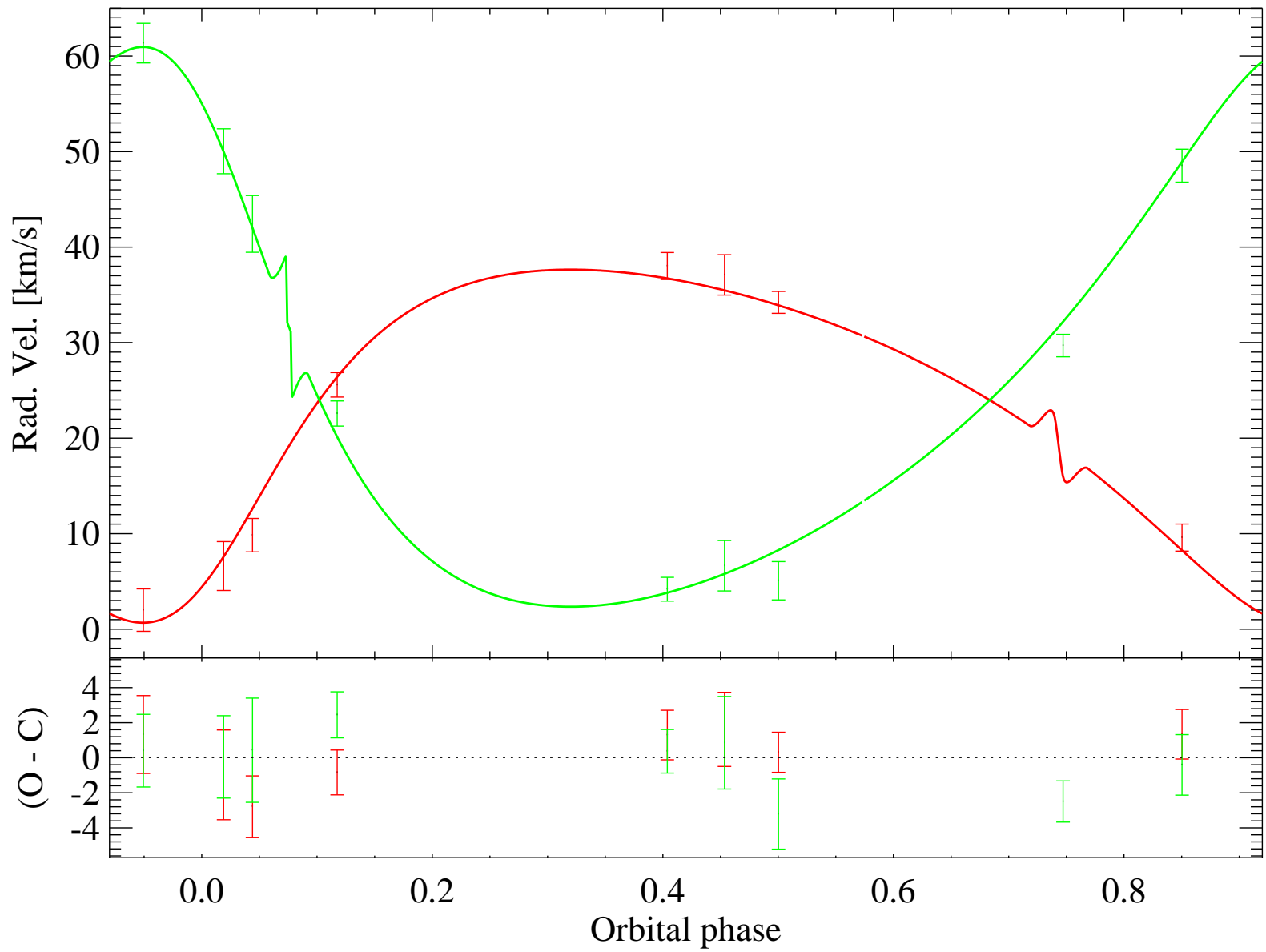
Fig. 5.— We use the COND atmosphere models of Allard et al. (2001) to check whether the non-blackbody spectra of brown dwarfs may explain the unexpected reversal of effective temperatures with mass in 2M0535–05. *Upper panel:* COND model spectra at the effective temperatures of the primary (green) and secondary (red) components of 2M0535–05 are compared with simple blackbodies of the same temperatures (dashed lines). Dotted vertical lines demarcate the approximate bandpass of the I_C filter used for our light-curve observations. *Bottom left:* The flux ratio of the COND models in the upper panel is shown relative to the blackbody flux ratio as a function of wavelength in the I_C band. Also shown is the I_C -band filter bandpass profile (dotted curve) and the bandpass-weighted mean COND-to-blackbody flux ratio (dashed line), which is 1.02 in this case; that is, the COND flux ratio is within 2% of the blackbody value. *Bottom right:* Same as *bottom left*, except showing the T_{eff} ratio implied by the COND flux ratio. The bandpass-weighted value is 1.069 (dashed line), within 0.5% of the value of 1.064 ± 0.004 found in our WD analysis (§2.3) using simple blackbodies. Note: This figure appears in color in the electronic version of the journal.

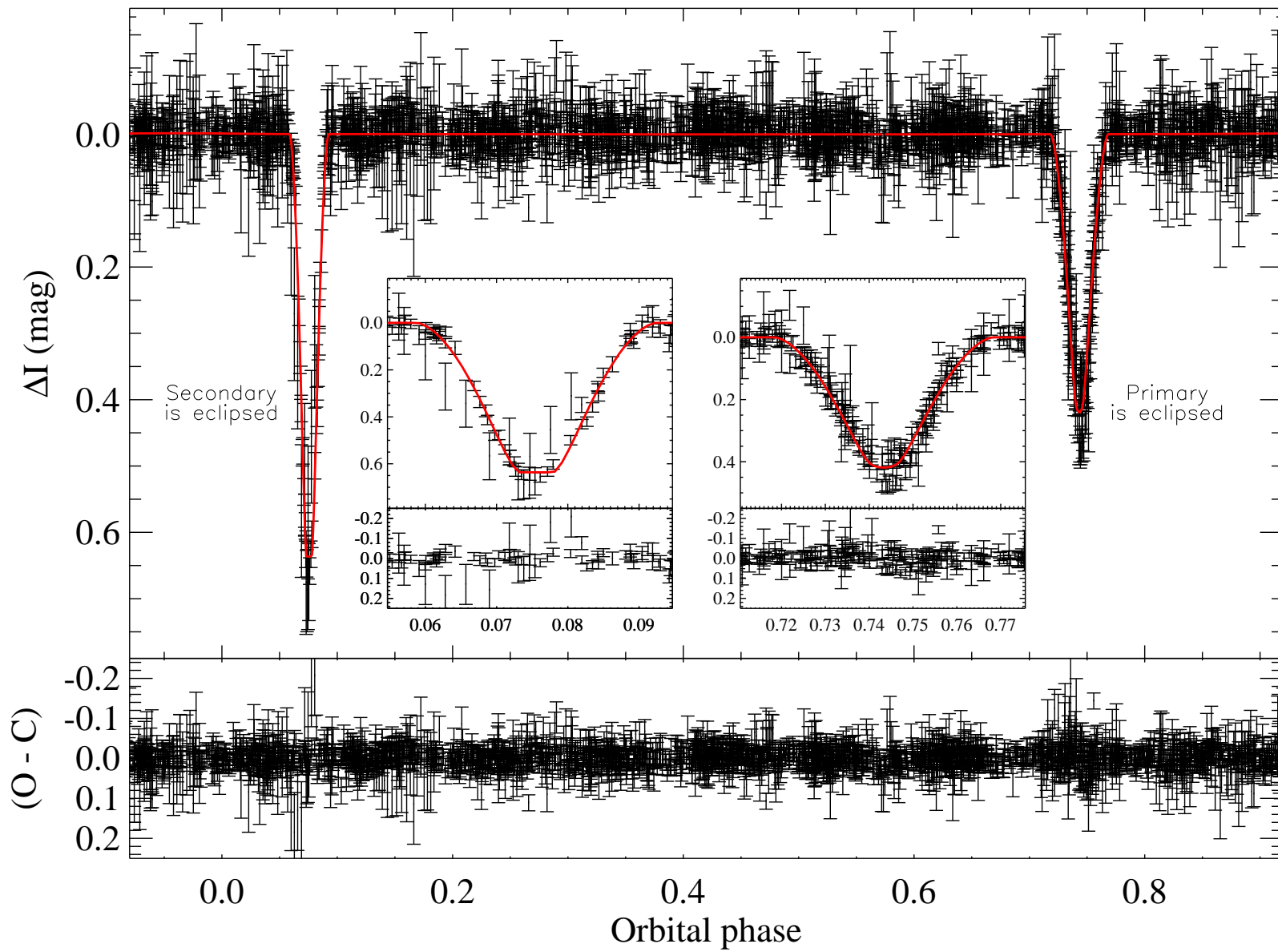
Fig. 6.— Comparisons of observations with theoretical models of young brown dwarfs. The measured radii,

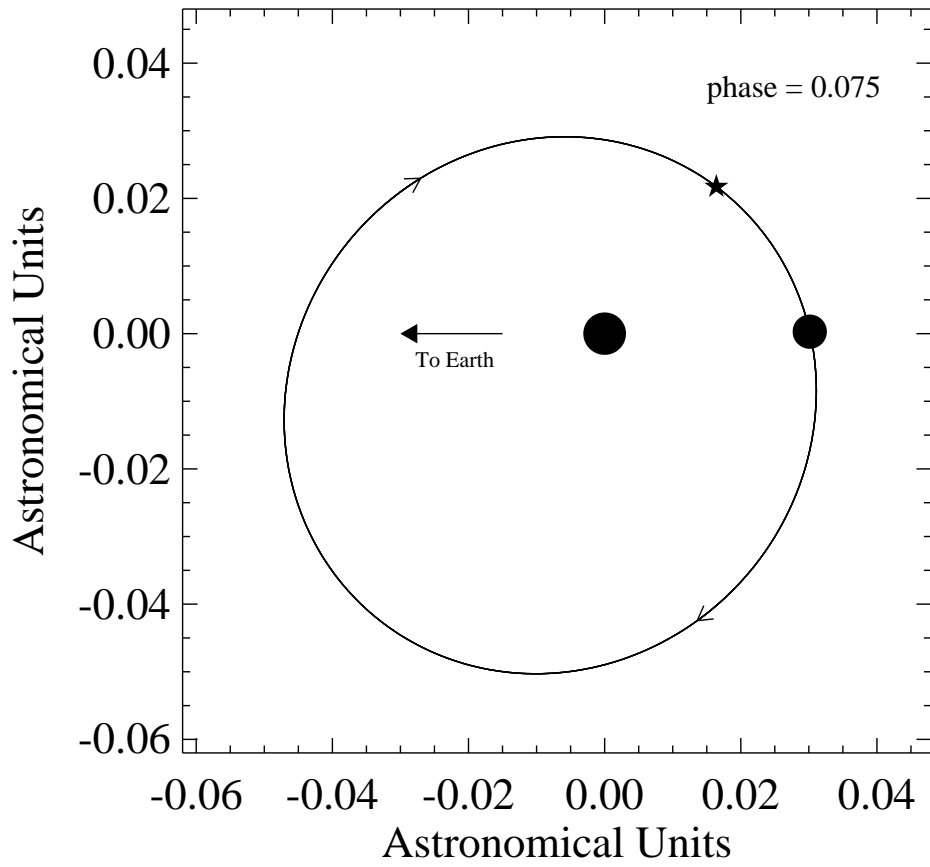
effective temperatures, and luminosities of 2M0535–05 (symbols with error bars) are compared to the values predicted by two sets of theoretical models (Baraffe et al. 1998; D’Antona & Mazzitelli 1997) of young brown dwarfs. Solid curves show the predicted evolution from 0.1 to 100 Myr for brown dwarfs with masses equal to those measured for the primary (green) and secondary (red) brown dwarfs in 2M0535–05. (The theoretical calculations of Baraffe et al. (1998) do not extend to ages less than 1 Myr.) Dashed curves bracketing the solid curves represent the 1σ measurement uncertainties in those masses. Observed and predicted values are generally in good agreement, particularly with the D’Antona & Mazzitelli (1997) models. Note that the effective temperature of the primary is predicted by both sets of models to be warmer than that of the secondary at any particular age, but that the D’Antona & Mazzitelli (1997) models allow the primary to be cooler than the secondary if it is sufficiently younger (see also Fig. 7). Note: This figure appears in color in the electronic version of the journal.

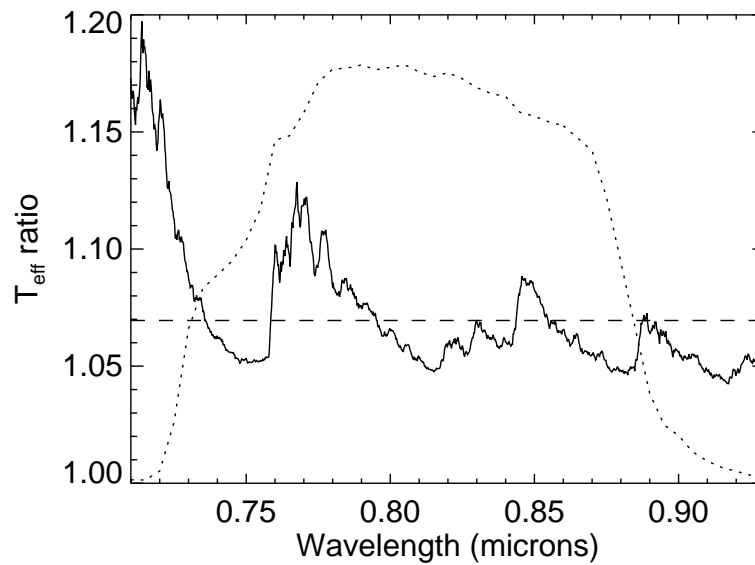
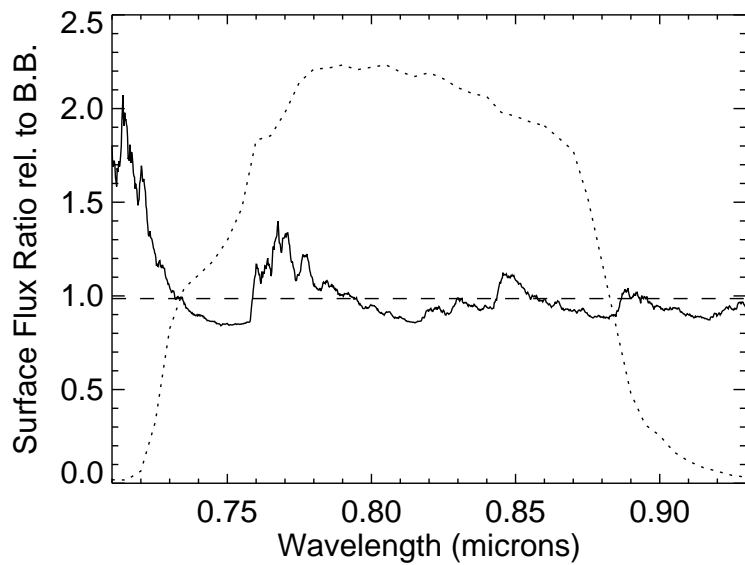
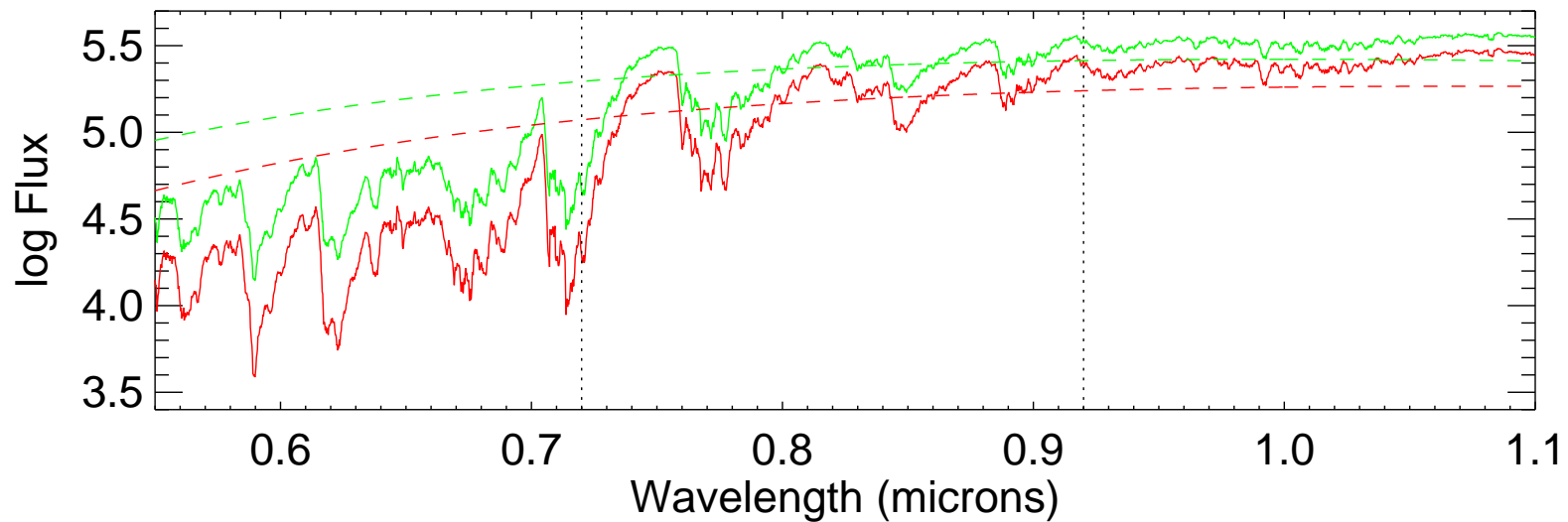
Fig. 7.— Same as Fig. 6, except with the 2M0535–05 components arbitrarily separated in age by 0.5 Myr ($\tau_1 = 0.75$ Myr, $\tau_2 = 1.25$ Myr). This demonstrates that the temperature reversal observed in 2M0535–05 may in fact be marginally consistent with the D’Antona & Mazzitelli (1997) models if the 2M0535–05 primary is taken to be slightly younger than the secondary. Note: This figure appears in color in the electronic version of the journal.



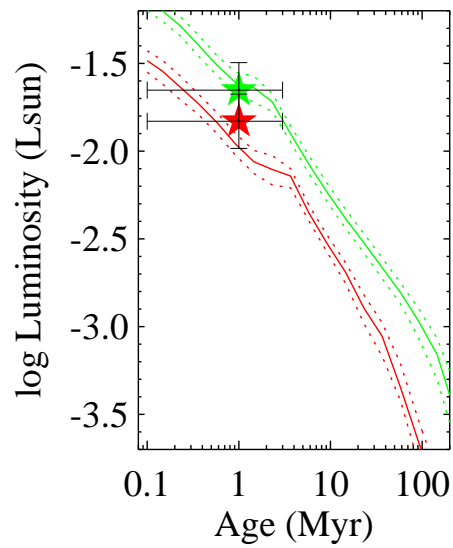
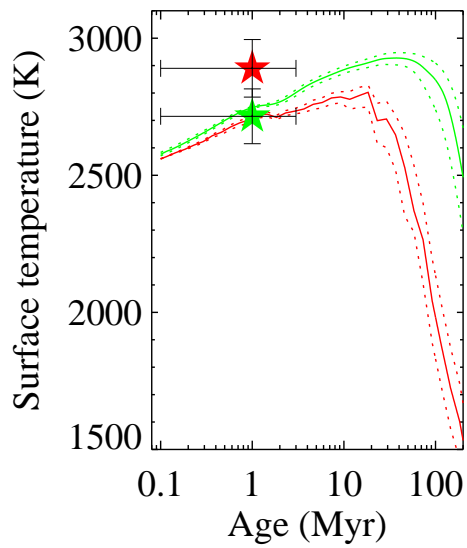
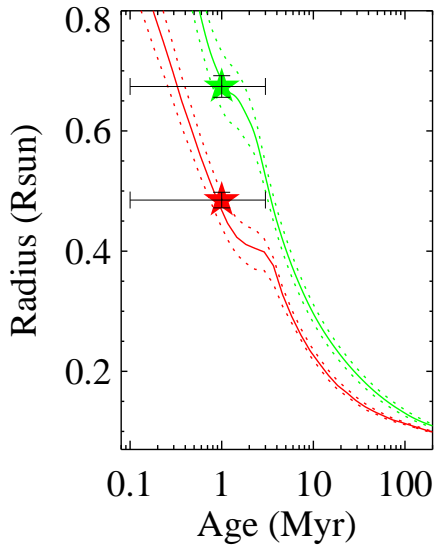




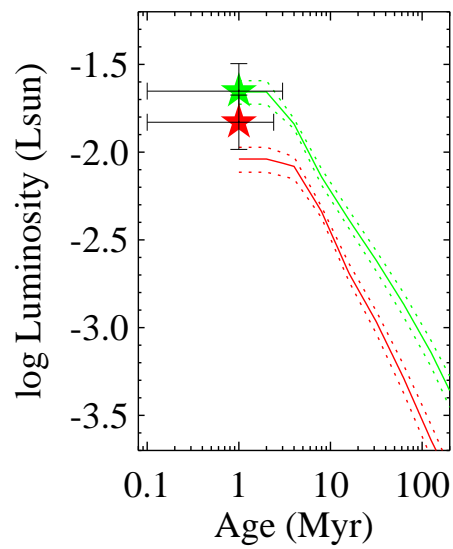
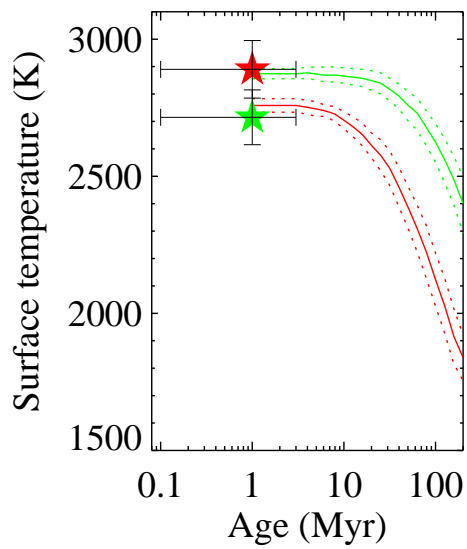
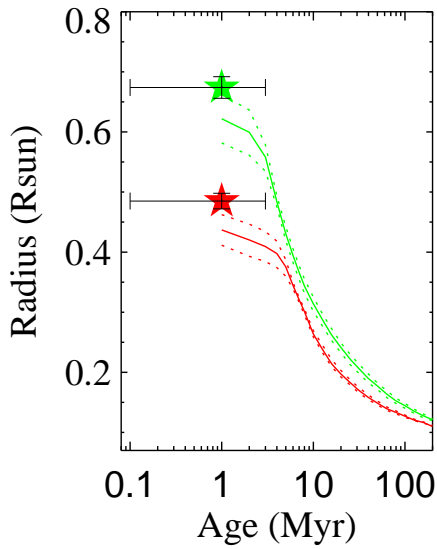




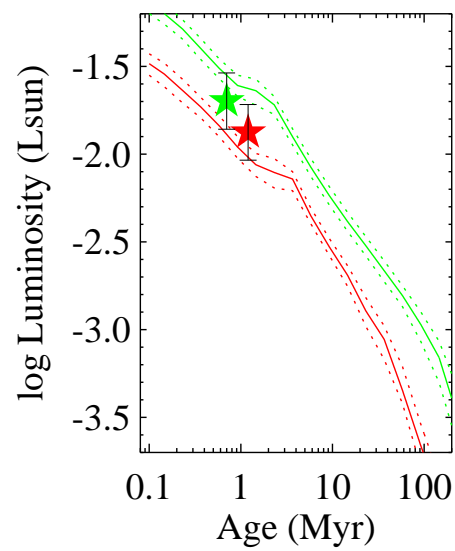
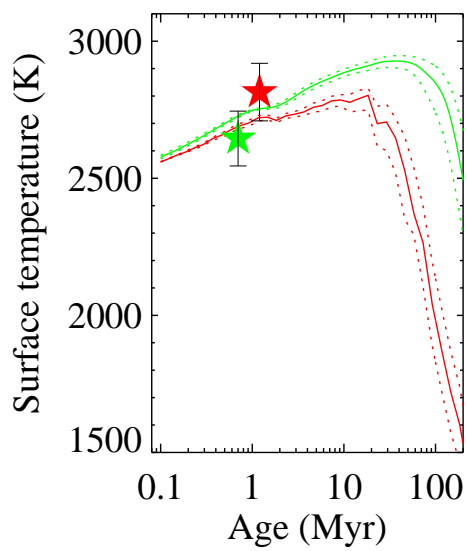
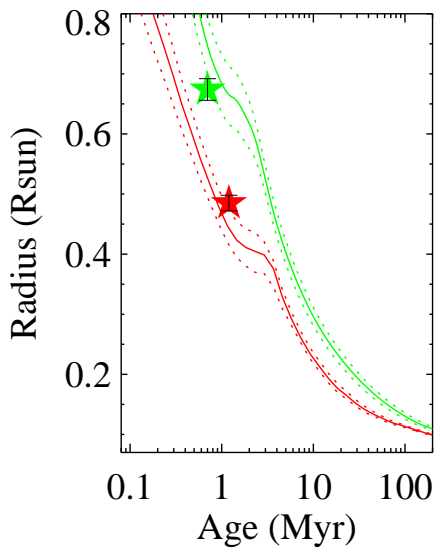
D'Antona et al. models



Baraffe et al. models



D'Antona et al. models



Baraffe et al. models

